EPD Congress 2004 *Edited by M.E. Schlesinger* ***TMS (The Minerals, Metals & Materials Society), 2004***

THE EFFECT OF SOLIDIFICATION PARAMETERS ON DENDRITE SPACING IN UNIDIRECTIONAL SOLIDIFICATION

Alicia E. Ares*, Rubens Caram**, and Carlos E. Schvezov ***

* University of Florida, Department of Materials Science and Engineering, 131 Rhines Hall,PO Box 116400, Gainesville, FL 32611-6400, USA.
** State University of Campinas, Materials Engineering Department, Campinas, São Paulo
C.P. 6122, 13083-970 BRASIL.
*** University of Misiones, Faculty of Sciences, 1552 Azara Street, Posadas, Misiones 3300, ARGENTINA.

Abstract

Experiments were carried out in which the conditions of dendritic growth are known, as well as the velocity and direction of solidification, in alloy systems such as Al-Cu, Al-Mg, Al-Zn, Al-Li, Al-Si, Al-Si-Cu, Cu-Zn, Pb-Sn, Sn-Pb and Steel. From these experiments it was determined that the primary dendritic spacing is a function of the temperature gradient, G, and the growth velocity, V, while the secondary and tertiary dendritic spacing are a function of the local solidification time, t_{SL}. In the present work, we investigated the relation proposed by Hunt, Kurz and Fisher and by An and Liu in such alloy systems with dendritic growth, besides that, we correlated secondary and tertiary measured dendritic spacings with the equations proposed by Kattamis et al., Allen and Hunt, Grugel and Feurer for the same alloy systems.

Introduction

The casting process, one of the most frequent method employed in the production of industrial parts, permits the fabrication of components with a high degree of geometrical complexity. Despite the fact that it is a very old technique, its scientific study started about half century ago and yet, some of the basic phenomena present during casting are not completely understood. One of the most basic and important phenomena is the formation of a given microstructure, which at the end define the properties of the cast part [1-2].

The formation of the microstructure occurring during solidification and the associated transformations, define the resulting grown morphology as well as the morphology and nature of many of the grown- in defects [3]. The study of the microstructures involve the determination of qualitative and quantitative parameters of the dendritic structure and phases present. The dendritic structure is the most frequent morphology of the solidifying interface during casting and the final structure [4]. The dendrites may consist of a complex array of primary, secondary, tertiary arms, end eventually higher order arms.

The importance of analyzing the dendritic growth is the relation with microsegregation and other defects [5]. The degree of microsegregation can be reduced by heat treatment; in such case, the diffusional distance become an important parameter; for alloys this dis-

tance is related to the dendritic dimensions, particularly the primary and secondary spacings. On the other hand, the effect of the microstructure on mechanical properties, it has been established that the continuity of the primary arms influence the ductility of the alloy and the secondary and tertiary arms define the spatial distribution of the eutectic and other phases, which may negatively affect the integrity of the component [6]. In other words, the morphology and dimensions of the dendritic structure are important in defining the properties of the cast alloys.

The development of a given dendritic structure is governed by many factors [7] which could be interrelated in complex forms and make the analysis difficult. In order to relate the dendritic spacings with both; the intrinsic properties of the alloy and the thermal conditions during solidification, a number of theoretical and empirical models have been elaborated, [8]. Some of the more relevant and employed in this research are presented next.

Primary dendrite spacing

The first best known and employed relation to predict the primary dendritic spacing λ_1 is due to Hunt [9], which can be written as follows:

$$\lambda_1 G^{1/2} V^{1/4} = 2.83 (D \Gamma \Delta T_0 / K)^{1/4} \quad (1)$$

where G is the temperature gradient in the liquid ahead of the dendrite tips, V is the velocity of the solidification front, D is the diffusivity of the solute in the liquid, Γ is a capillarity parameter ($\sigma/\Delta S$, where σ is the interfacial solid-liquid free energy and ΔS is the entropy of fusion), k is the partition coefficient of the solute and ΔT_0 is the range of cooling of the alloy. The values predicted by the above equation showed reasonable correlation with the experimental results

Kurz and Fisher [10] developed a similar relation to equation (1) which is given as follows:

$$\lambda_1 G^{1/2} V^{1/4} = 4.3 (D \Gamma \Delta T_0 / K)^{1/4} \quad (2)$$

the predicted values of λ_1 are $(1.51/k)^{1/2}$ times larger than those predicted by equation (1). They have also shown that equation (2) overestimates the values of λ_1 with respect to the measured values for aluminum alloys containing Al-2.4, 4.4 and 10.1 wt% Cu (% in weight) [11]. In fact, it has been established that [12-15] the measured spacings are within the values predicted by equations (1) and (2).

Trivedi [13] has developed a more complex model with results which were in good agreement with the experimental results for succinonitrile - 5 mol % acetone. A simplified version of the model due to An and Liu [14] resulted in the following relation:

$$\lambda_1 G^{1/2} V^{1/4} = A (D \Gamma k \Delta T_0)^{1/4} \quad (3)$$

where A is between 4.23 and 7.09.

Secondary dendrite spacing

It has been shown that the main parameter which defines the secondary arm spacing is the local solidification time defined as;

$$t_{SL} = \frac{\Delta T}{GV} \tag{4}$$

where ΔT is the difference between the liquidus and solidus temperatures. In general, the spacing and time has been related through an equation of the type:

$$\lambda_2 = K_1 * t_{SL}^{\ a} \tag{5}$$

where a and K_1 are parameters associated to the particular alloy system. One of the first studies on the subject is due to Kattamis, et al. [16] who found that the dendrite arms with larger curvature grow at the expense of the remelting of the arms with smaller curvature. Based on this observation Feurer [6] developed a model which predicts the secondary spacing λ_2, by means of the following equation:

$$\lambda_2 = 4.36\,(\overline{M}\, t_L)^{1/3} \tag{6}$$

where $\overline{M}$ is a coarsening parameter calculated as follows:

$$\overline{M} = \frac{2\sigma_{sl} T_l D_l \ln(C_E / C_0)}{Hm(1-k_0)(C_E - C_0)} \tag{7}$$

where σ_{sl} is the solid/liquid surface tension, T_l is the liquidus temperature, D_l is the diffusivity of the solute, C_E is the eutectic composition, C_0 is the nominal composition of the alloy, H is the latent heat of fusion, m is the slope of the liquidus line and k_0 is the partition coefficient. According to equation (7), the thermophysical parameters and the nature and composition of the alloy play important roles in defining the secondary dendrite spacing.

In another development, Grugel [8], from experimental results in Al-Si alloys containing 4, 6, 8, 10 and 12 % Si (weight %), determined that the secondary spacing, λ_2, considering only the active branches can be calculated as:

$$\lambda_2 = 10\,(t_{SL})^{1/2} \tag{8}$$

where t_{SL} is in seconds and λ_2 in μm.

Tertiary dendrite spacing

There are few studies available on tertiary dendrite spacing, two of them are particularly mentioned here; one due to Grugel [8] and another due to Taha [18]. Grugel [8] concluded that the tertiary arms coarsened similarly to the secondary arms, resulting in a spacing which follows the equation:

$$\lambda_3 = 10\,(t_{SL})^{1/3} \tag{9}$$

where, t_{SL} is in seconds and λ_3 in μm.

In the present report, and from experimentally determined values, the effect of the different solidification parameters like gradient, velocity and local solidification time are correlated with the primary, secondary and tertiary dendrite spacings in a variety of alloy systems and compositions.

Experimental

The alloys were prepared from pure materials of different grades, and the samples were solidified directionally upwards in a furnace which was described elsewhere [19]. During each experiment the temperatures were measured with K-type thermocouples calibrated and inserted in the cylindrical container at different distances from the base of the sample.

The microstructure was characterized using an image analyser coupled to an optical microscope. The sample was sectioned in the longitudinal direction and one of the halves was then cut in the perpendicular direction to the axis at different distances from the base of the solidfied sample. The cross sections were mounted, polished and etched [20] for observation. The measurements of spacings were done using the line intersect technique, preferentially in regions near thermocouple positions for a closer correlation with the solidification parameters.

Results

Primary dendrite spacing

The complete set of experimental results on λ_1 is listed in Table I. In the same table is included the data collected from other authors which are employed in the present research [11-15,21-24]. The values of $\lambda_1 G^{1/2} V^{1/4}$ are between 10 and 221 $\mu m^{3/4} K^{1/2} s^{-1/4}$. The correlation between λ_1 and $G^*V^{1/2}$ does not show a strong dependance with alloy concentration for each alloy system, as can be observed in Table I. The data from Table I and the complete set of the measured values are plotted in Figures 1 to 8. The line in each figure are drawn for values of $\lambda_1 G^{1/2} V^{1/4}$ of 88.25 ± 6.5, 22.07 ± 1.5, 21.23 ± 2.5, 63.24 ± 9, 138.32 ± 15, 30.5 ± 6, 29.66 ± 4, 71.09 ± 8 $\mu m^{3/4} K^{1/2} s^{-1/4}$, respectively with each figure from 1 to 8 which are valid in the following ranges; $0.00005 < G^*V^{1/2} < 1.48$ K $\mu m^{1/2}\, s^{-1/2}$ and $20 < \lambda_1 < 1150$ µm.

Table I. Experimental values of λ_1 as function of G and V for the different alloy systems.

Alloy (wt %)	Range of λ_1 (µm)	Range of G (K/µm)	Range of V (µm/s)	$\lambda_1 G^{1/2} V^{1/4}$ ($\mu m^{3/4} K^{1/2} s^{-1/4}$)	
				(present work)	(previous)
Al-2%Cu	105-530	0.0001-0.002	200-2500	22 ± 9	58 ± 6 [11]
Al-4%Cu	192-750	0.00002-0.0015	200-1700	34 ± 5	54 ± 8 [11]
Al-10%Cu	70-540	0.0002-0.0025	700-4500	76 ± 4	62 ± 8 [11]
Al-20%Cu	30-1000	0.0002-0.0015	900-4200	221 ± 8	52 ± 11 [18]
Al-2%Mg	40-900	0.0001-0.0003	400-1000	33 ± 2	-------
Al-4%Mg	30-360	0.0001-0.0005	200-1000	11 ± 1	-------
Al-2%Zn	100-1100	0.0001-0.0004	300-1200	10 ± 2	-------

Al-4%Zn	70-400	0.0002-0.0004	200-1000	11 ± 3	-------
Al-5%Si	30-545	0.00005-0.0017	100-900	58 ± 11	87 ± 11 [15]
Al-7%Si	50-700	0.00035-0.027	200-1000	105 ± 16	92 ± 10 [24]
Al-10%Si	20-400	0.0001-0.036	200-1000	58 ± 8	74 ± 8 [24]
Al-10%Si-2.5%Cu	30-1150	0.0001-0.0025	100-1100	61 ± 6	59 ± 7 [21]
Al-5%Si-12%Al_2O_3	70-480	0.00005-0.001	300-900	34 ± 5	-------
Cu-36%Zn-2.8%Pb	30-840	0.0001-0.02	200-5500	138 ± 15	-------
Pb-2%Sn	30-300	0.00005-0.017	10-500	45 ± 7	-------
Pb-4%Sn	20-390	0.00005-0.007	10-500	18 ± 3	-------
Pb-10%Sn	40-320	0.00005-0.007	10-500	22 ± 6	9 ± 2 [22]
Pb-20%Sn	100-270	0.0005-0.0025	10-500	38 ± 7	11 ± 2 [22]
Pb-30%Sn	80-250	0.0005-0.0045	10-500	39 ± 7	30 ± 5 [22]
Pb-40%Sn	50-200	0.0001-0.0057	10-500	21 ± 4	28 ± 6 [22]
Sn-2%Pb	30-350	0.00005-0.008	20-300	14 ± 3	15 ± 4 [23]
Sn-4%Pb	40-270	0.0009-0.0016	20-300	20 ± 3	-------
Sn-10%Pb	22-370	0.0002-0.004	20-300	55 ± 6	-------
Acero 316 L	30-900	0.0001-0.001	910-4·10^4	71 ± 8	-------

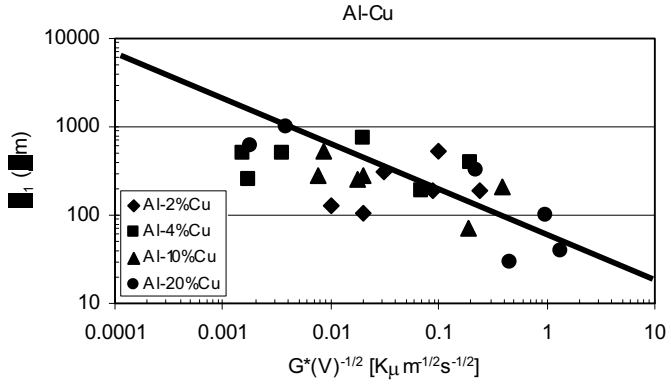

Figure 1. Primary dendrite spacing, λ_1, as a function of $G^*V^{1/2}$ for Al-2%Cu, Al-4%Cu, Al-10%Cu and Al-20%Cu (wt %). Full line indicates $\lambda_1 G^*V^{1/2} = 88.25\ \mu m^{3/4}K^{1/2}s^{-1/4}$.

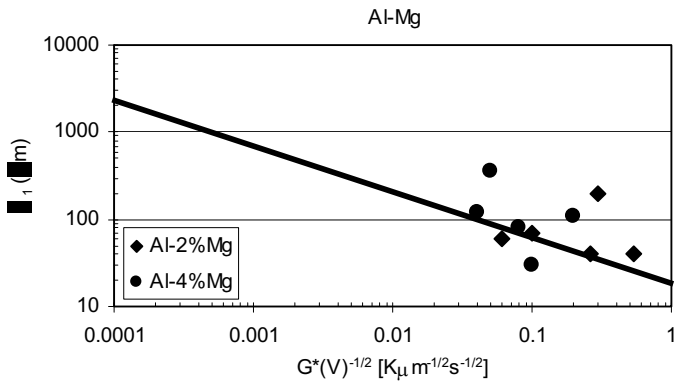

Figure 2. Primary dendrite spacing, λ_1, as a function of $G^*V^{1/2}$ for Al-2%Mg and Al-4%Mg (wt %). Full line indicates $\lambda_1 G^*V^{1/2} = 22.07\ \mu m^{3/4}K^{1/2}s^{-1/4}$.

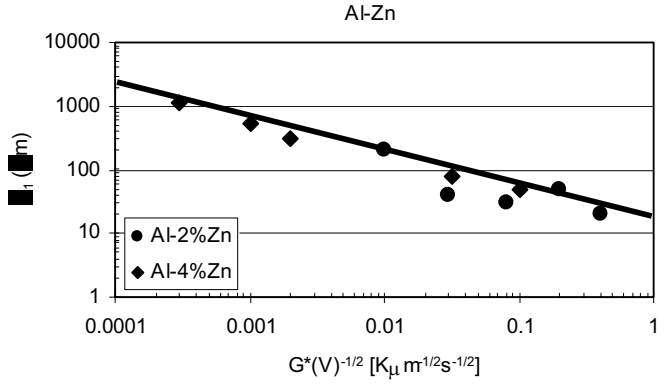

Figure 3. Primary dendrite spacing, λ_1, as a function of $G^*V^{1/2}$ for Al-2%Zn and Al-4%Zn (wt %). Full line indicates $\lambda_1 G^*V^{1/2} = 21.23\ \mu m^{3/4}K^{1/2}s^{-1/4}$.

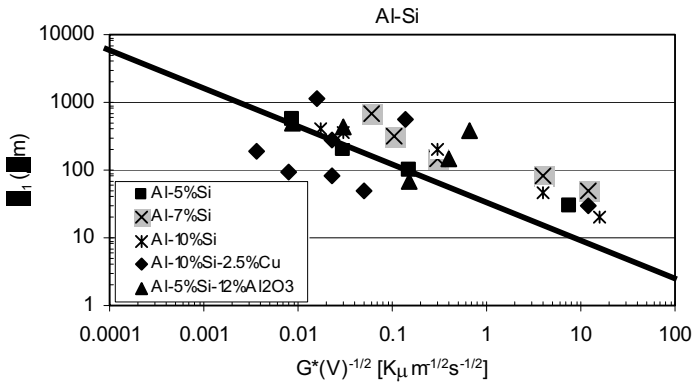

Figure 4. Primary dendrite spacing, λ_1, as a function of $G^*V^{1/2}$ for Al-5%Si, Al-7%Si, Al-10%Si, Al-10%Si-2.5%Cu and Al-5%Si-12%Al_2O_3 (wt-%). Full line indicates $\lambda_1 G^*V^{1/2} = 63.24\ \mu m^{3/4}K^{1/2}s^{-1/4}$.

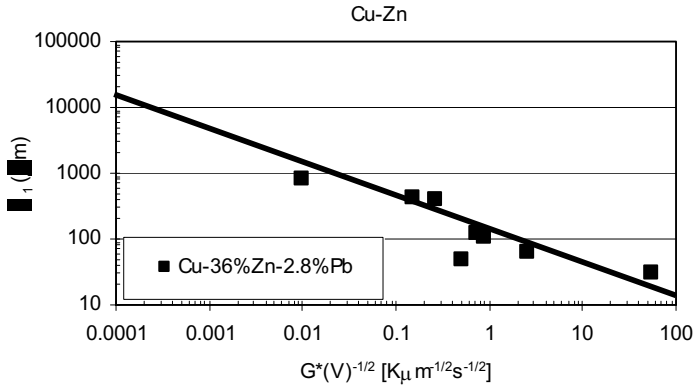

Figure 5. Primary dendrite spacing, λ_1, as a function of $G^*V^{1/2}$ for Cu – 36%Zn - 2.8%Pb (wt %). Full line indicates $\lambda_1 G^*V^{1/2} = 138.32\ \mu m^{3/4}K^{1/2}s^{-1/4}$.

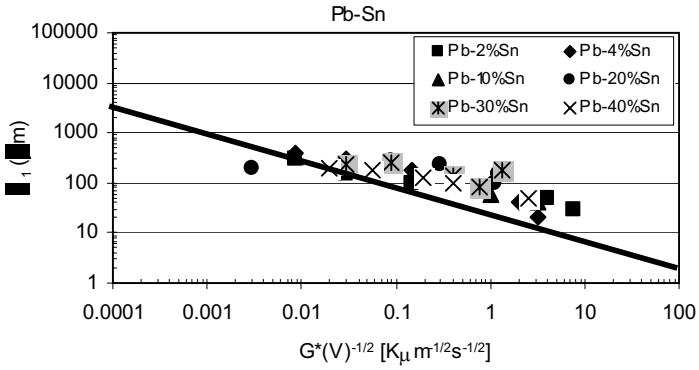

Figure 6. Primary dendrite spacing, λ_1, as a function of $G^*V^{1/2}$ for Pb-2%Sn, Pb-4%Sn, Pb-10%Sn, Pb-20%Sn, Pb-30%Sn and Pb-40%Sn, (wt %). Full line indicates $\lambda_1 G^*V^{1/2} = 30.50\ \mu m^{3/4}K^{1/2}s^{-1/4}$.

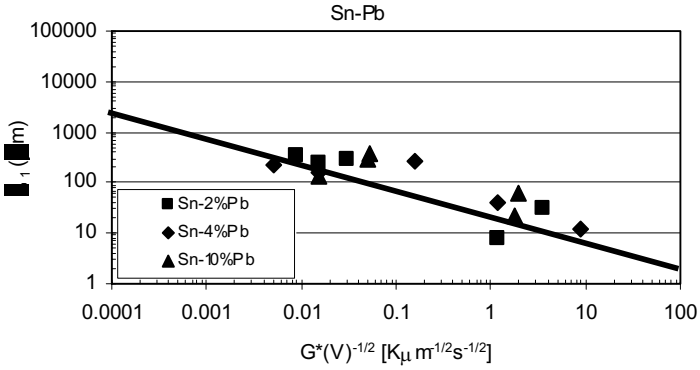

Figure 7. Primary dendrite spacing, λ_1, as a function of $G^*V^{1/2}$ for Sn-2%Pb, Sn-4%Pb and Sn-10%Pb (wt %). Full line indicates $\lambda_1 G^*V^{1/2} = 30.50\ \mu m^{3/4}K^{1/2}s^{-1/4}$.

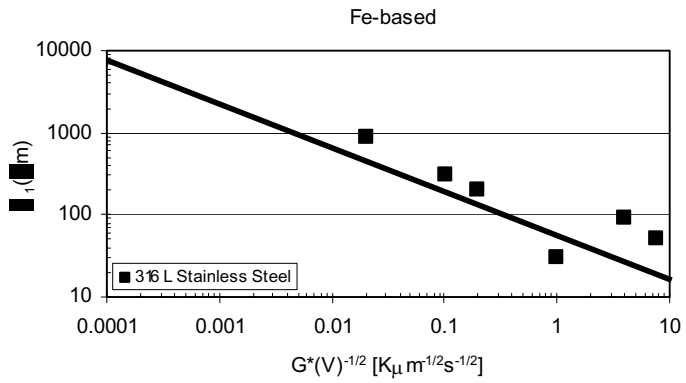

Figure 8. Primary dendrite spacing, λ_1, as a function of $G^*V^{1/2}$ for 316 L Stainless Steel (Fe-16.6%Cr-10.1%Ni-0.03%C-1.40%Mn-2.20%Mo-0.47%Si, wt.-%). Full line indicates $\lambda_1 G^*V^{1/2} = 71.9 \mu m^{3/4} K^{1/2} s^{-1/4}$.

Secondary dendrite spacing

The main solidification parameters necessary for the analysis are the growth velocity and the temperature gradient. They are calculated as:

$$V = \frac{2\,cm}{\Delta t} \tag{7}$$

and

$$G = \frac{\Delta T}{2\,cm} \tag{8}$$

where Δt is the time taken for the interphase (liquid or solid) to pass two consecutive thermocouple positions, ΔT is the temperature difference between the same thermocouples and 2 cm is the separation distance between each pair of thermocouples.

The measured secondary arm spacing include active and inactive arms. The results were compared with predictions from two models; the theoretical model due to Feurer [6] and the empirical model due to Grugel [8]. In the case of the Feurer model, the thermophysical parameters and data for each alloy system were taken from the literature. Using these data the coefficient relating λ_2 and t_{SL},for each alloy, was calculated and resulted in the equations which are listed in Table 2. The results were also compared with the empirical equation (8) due to Grugel. Both equations were plotted for each alloy system and composition, together with the experimental measurements; they are presented as Figure 9. In the figure it can first be observed that in all cases, an increase in the local solidification time produce an increase in the secondary spacing. However, when the predictions are considered, it is observed that the best fit between experimental results and predictions is achieved with the coefficients and functional dependence given by the Feurer model, while the Grugel model predicts spacings well above the experimental values. Moreover, it can be concluded that in no case the secondary spacing follow a square root law of the local solidification time.

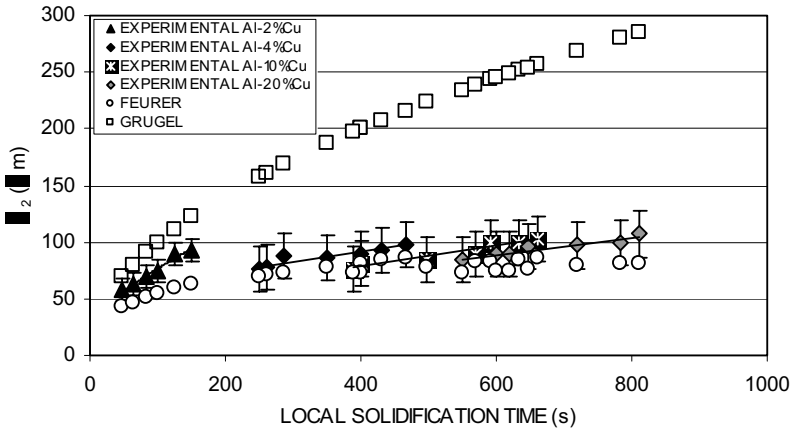
EXPERIMENTAL Al-2%Cu
EXPERIMENTAL Al-4%Cu
EXPERIMENTAL Al-10%Cu
EXPERIMENTAL Al-20%Cu
FEURER
GRUGEL
λ2 (μm)
LOCAL SOLIDIFICATION TIME (s)

(a)

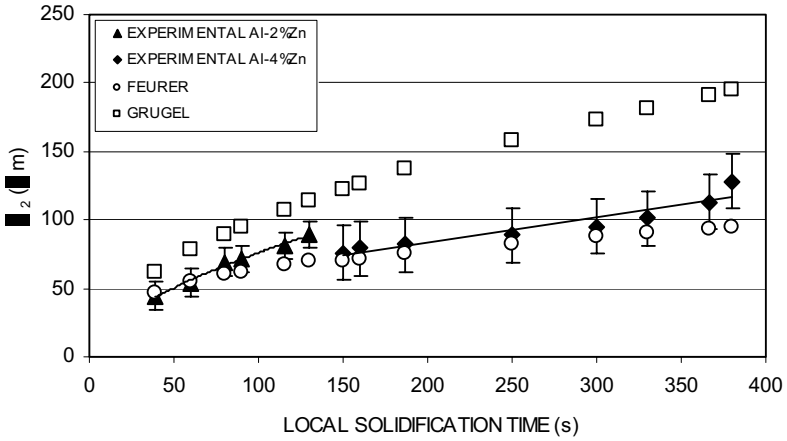
EXPERIMENTAL Al-2%Zn
EXPERIMENTAL Al-4%Zn
FEURER
GRUGEL
λ2 (μm)
LOCAL SOLIDIFICATION TIME (s)

(b)

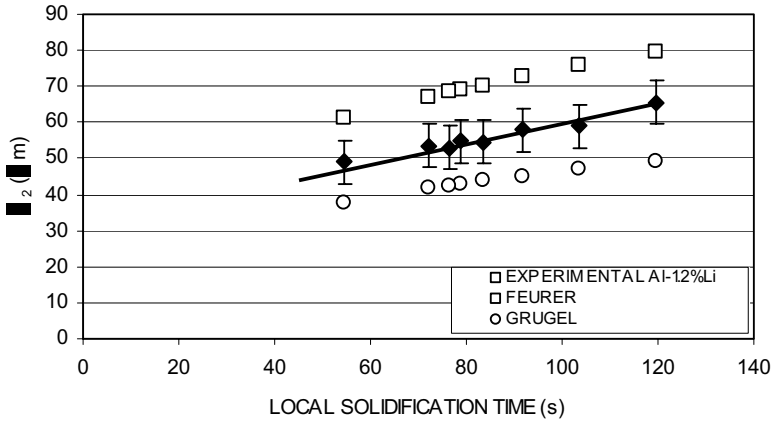
EXPERIMENTAL Al-1.2%Li
FEURER
GRUGEL
λ2 (μm)
LOCAL SOLIDIFICATION TIME (s)

(c)

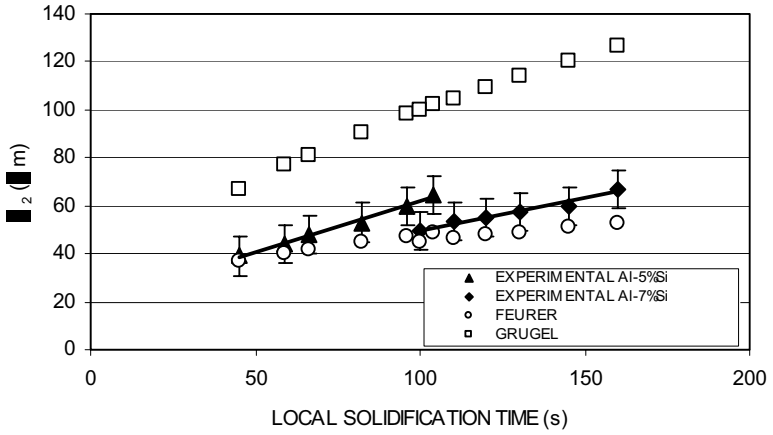

(d)

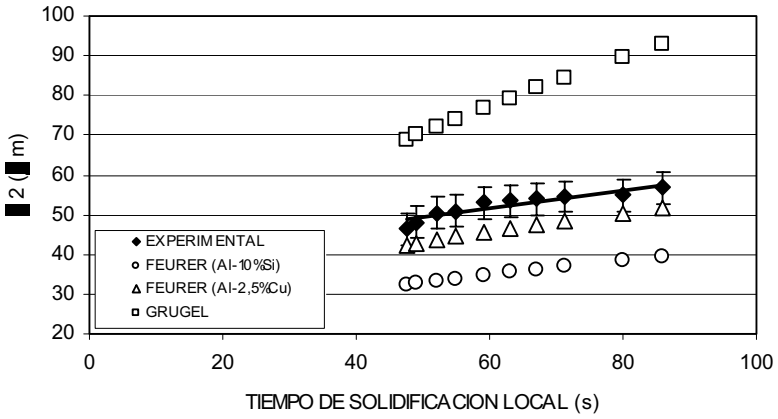

(e)

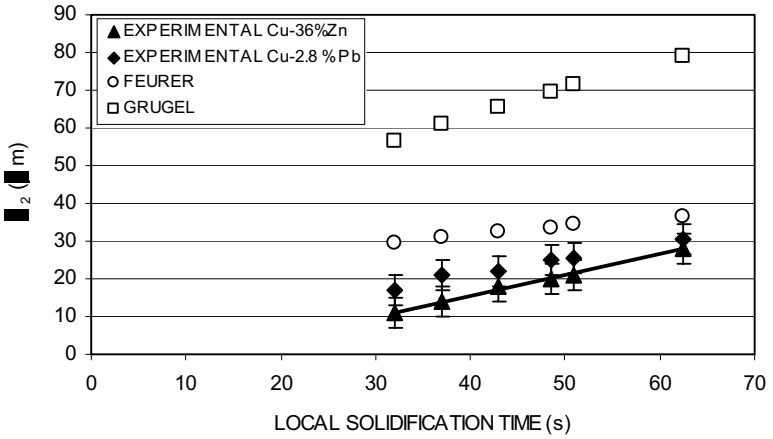

(f)

Figure 9. Influence of the local solidification time on the secondary dendritic growth experimentally obtained and compared with the results from theoretical and empirical models. (a) Al-Cu, (b)Al-Zn (c) Al-Li (d) Al-Si, (e) Al-Si-Cu. (f) Cu-Zn-Pb.

Table 2. Equations obtained for the secondary spacing using the Feurer model [6] for the different alloy systems.

Alloy	**Feurer Equation**
Al-2%Cu	$\lambda_2 = 11.9 * t_{SL}^{1/3}$
Al-2.5%Cu	$\lambda_2 = 11.7 * t_{SL}^{1/3}$
Al-4%Cu	$\lambda_2 = 11.1 * t_{SL}^{1/3}$
Al-10%Cu	$\lambda_2 = 9.8 * t_{SL}^{1/3}$
Al-20%Cu	$\lambda_2 = 8.8 * t_{SL}^{1/3}$
Al-2%Zn	$\lambda_2 = 13.9 * t_{SL}^{1/3}$
Al-4%Zn	$\lambda_2 = 13.1 * t_{SL}^{1/3}$
Al-5%Si	$\lambda_2 = 10.3 * t_{SL}^{1/3}$
Al-7%Si	$\lambda_2 = 9.7 * t_{SL}^{1/3}$
Al-10%Si	$\lambda_2 = 8.9 * t_{SL}^{1/3}$
Al-1.2%Li	$\lambda_2 = 16.1 * t_{SL}^{1/3}$
Cu - 36%Zn-2.8%Pb	$\lambda_2 = 9.2 * t_{SL}^{1/3}$

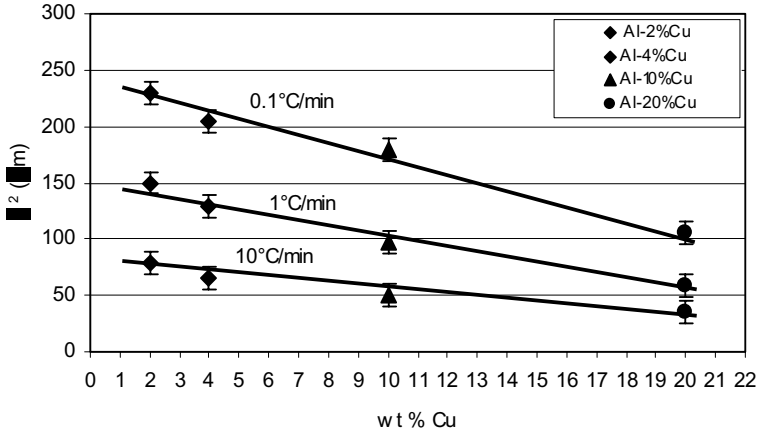

Figure 10. Effect of copper solute content on secondary dendrite arm spacing in four aluminum alloys, as plotted for three different cooling rates.

The effect of cooling rate and alloy composition on secondary spacing can be observed in Figure 10 for aluminum-copper alloys. In the figure, the secondary spacing is presented as a function of copper concentration for three different cooling rates, covering three different orders of magnitude; 0.1, 1 and 10°C/min. In the three cases the secondary spacing decreases linearly with concentration, with slopes that decrease with increasing cooling rates. This is indicating that the effect of concentration is stronger for slower cooling rates. On the other hand, for a given concentration, the spacing increases as the cooling

rate decreases, however not in a linear relation. These results are in agreement with those obtained by Howard and Mondolfo as mentioned in reference 15 for the same alloy systems.

Tertiary dendrite spacing

The measured tertiary dendrite spacings were plotted as function of in Figure 11, for the three alloy systems; Al-Cu, Al-Si and Al-Si-Cu. In the same figure it is plotted the relation between spacing and time as proposed by Grugel, and given by equation 9. It is observed that an increase in local solidification time produce a decrease of spacing following a law which fits reasonably well with the cubic root of time as given by the Grugel model. In addition, it is observed that the functions that best fit the experimental results for both the secondary and tertiary dendrite spacings, are of the type of the third root of time.

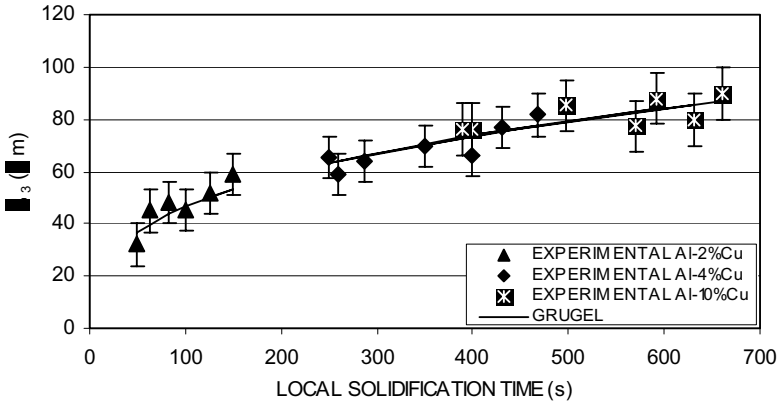

(a)

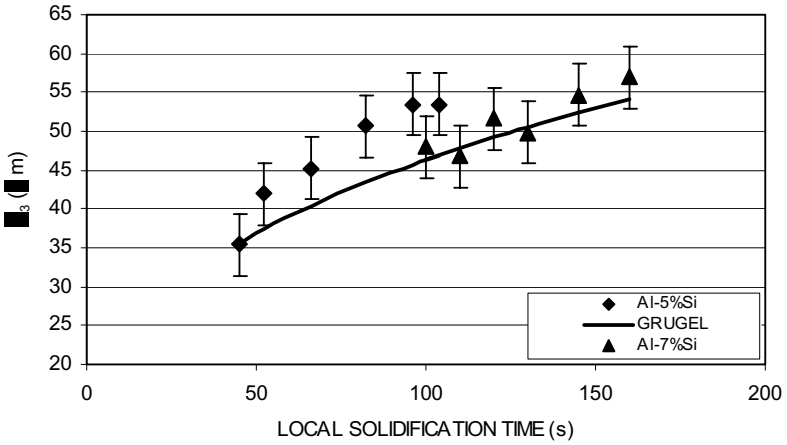

(b)

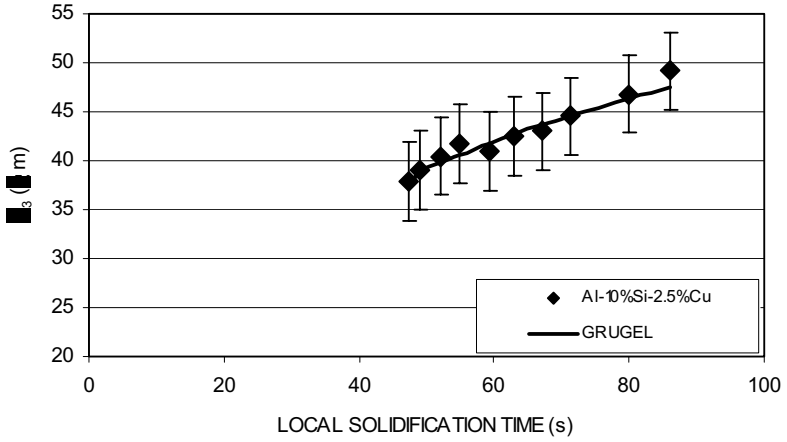

(c)

Figure 11. Local solidification time influence on the tertiary dendritic growth experimental obtained and compared with the results from Grugel model. (a) Al-Cu, (b) Al-Si, (c) Al-Si-Cu.

Conclusions

1. The experimental measurements of primary dendritic spacing, λ_1, are in good correlation with the temperature gradient, G, and growth velocity, V, through a relation of the type, $\lambda_1 \propto G^{-1/2} \times V^{-1/4}$, with values of $\lambda_1 G^{1/2} V^{1/4}$ in the range 10-221 $\mu m^{3/4} K^{1/2} s^{-1/4}$, but mostly in the range 20-60 $\mu m^{3/4} K^{1/2} s^{-1/4}$. The effect of alloy composition is within the scatter of experimental results.

2. The secondary and tertiary dendrite spacings increase with an increase in the local solidification time.

3. The Feurer model (6) predicts the secondary spacing as a function of local solidification time in good agreement with the experimental results. The Grugel model (8) predicts values well above the experimental values.

4. The tertiary dendrite spacing is well described by the Grugel model (8).

5. For the Al-Cu system, as the Copper concentration increases, the secondary dendrite spacing decreases for a given cooling rate. On the other hand, for a given concentration, an increase in the cooling rate produce a decrease in the secondary dendrite spacing. The results are in agreement with those reported by Horwath and Mondolfo (15) in Al-Cu alloys.

Acknowledgements

Thanks are due to the Argentinean Research Council (CONICET) and Brazilian Research Council (FAPESP) for the financial support.

References

1. W. Kurz, D.J. Fisher, Fundamentals of Solidification, Switzerland, 3° ed., Trans. Tech. Publications, 305 (1989).

2. M.H. McKay, T.D. McKay, J.A. Hopkins, Metall Trans. B, 24 (1993) 669.

3. A.M. Samuel, F.H. Samuel, J. Materials Science, 30 (1995) 4823.

4. W. Kurz, R. Trivedi, Acta Metall. Mater., 38 (1990) 1.

5. S.C. Huang, M.E. Glicksman, Acta Metallurgica, 29 (1981) 701.

6. U. Feurer, in: The Symposium on Quality Control of Engineering Alloys, Delft, 131 (1977).

7. R. Trivedi, W. Kurz, International Materials Reviews, 39 (1994) 49.

8. R.N. Grugel, J. Materials Science, 28 (1993) 677.

9. J.D. Hunt, in: Solidification and Casting of Metals (The Metals Society, London, 1979) p.p. 3-9.

10. W. Kurz and J.D. Fisher, Acta Metall. 29 (1981) 11.

11. K.P. Young and D.H. Kirkwood, Metall. Trans. A 6 (1975) 197.

12. H. Jones and W. Kurz, Metall. Trans. A 11 (1980) 1265.

13. R. Trivedi, Metalls. Trans. A 15 (1984) 977.

14. G. An and L. Liu, J.Crystal Growth 80 (1987) 383.

15. S.A. Moir and H. Jones, J. Crystal Growth, in press.

16. T.Z. Kattamis, J.C. Couglin, M.C. Flemings, Trans. AIME, 239 (1967) 1504.

17. D.J. Allen, J.D. Hunt, Metall. Trans. A, 7 (1976) 767.

18. M.A. Taha, Metals Science, 9 (1979) 9.

19. A.E. Ares, C.T. Rios, R. Caram, C.E. Schvezov, "Columnar-to-Equiaxed Transition in 316 L Stainless Steel" EPD Congress 2002, Edited P.R. Taylor, Fundamentals of Advanced Materials for Energy Conversion, Edited by D. Chandra and R.G. Bautista, TMS (The Minerals, Metals & Materials Society) (2002) 567-582.

20. G. Kehl, Fundamentos de la Práctica Metalográfica, Editorial Aguilar, Madrid (1963).

21. C.T. Rios, R. Caram, J Crystal Growth 174 (1997) 65-69.

22. J.A. Spittle and D.M. Lloyd, in: Solidification and Casting of Metals (The Metals Society, London, 1979) p.p. 15-20.

23. J.A. Bell and W.C. Winegard, J. Inst. Metall. 92 (1963/64) 357.

24. R.N. Grugel, J Mater. Sci. 28 (1993) 677.